2011

Quasi-Degenerate Second-Order Perturbation Theory for Occupation Restricted Multiple Active Space Self-Consistent Field Reference Functions

Luke Roskop
Iowa State University, lukebr@iastate.edu

Mark S. Gordon
Iowa State University, mgordon@iastate.edu

Quasi-Degenerate Second-Order Perturbation Theory for Occupation Restricted Multiple Active Space Self-Consistent Field Reference Functions

Abstract
A multi-configuration quasi-degenerate second-order perturbation method based on the occupation restricted multiple active space (ORMAS-PT/ORMAS) reference wavefunction is presented. ORMAS gives one the ability to approximate a complete active space self-consistent field (CASSCF) wavefunction using only a subset of the configurations from the CASSCF space. The essential idea behind ORMAS-PT is to use the multi-reference Møller-Plesset formalism to correct the ORMAS reference energy. A computational scheme employing direct CI methodology is presented. Several tests are presented to demonstrate the performance of the ORMAS-PT method.

Keywords
Subspaces, Wave functions, Polymers, Perturbation theory, Buckling

Disciplines
Chemistry

Comments
The following article appeared in *Journal of Chemical Physics* 135 (2011): 044101, and may be found at doi:10.1063/1.3609756.

Quasi-degenerate second-order perturbation theory for occupation restricted multiple active space self-consistent field reference functions

Luke Roskop and Mark S. Gordon

Citation: The Journal of Chemical Physics **135**, 044101 (2011); doi: 10.1063/1.3609756
View online: http://dx.doi.org/10.1063/1.3609756
View Table of Contents: http://scitation.aip.org/content/aip/journal/jcp/135/4?ver=pdfcov
Published by the AIP Publishing

Quasi-degenerate second-order perturbation theory for occupation restricted multiple active space self-consistent field reference functions

Luke Roskop and Mark S. Gordon[a)]
Department of Chemistry, Iowa State University, Ames, Iowa 50010, USA

(Received 3 February 2011; accepted 20 June 2011; published online 22 July 2011)

A multi-configuration quasi-degenerate second-order perturbation method based on the occupation restricted multiple active space (ORMAS-PT/ORMAS) reference wavefunction is presented. ORMAS gives one the ability to approximate a complete active space self-consistent field (CASSCF) wavefunction using only a subset of the configurations from the CASSCF space. The essential idea behind ORMAS-PT is to use the multi-reference Møller-Plesset formalism to correct the ORMAS reference energy. A computational scheme employing direct CI methodology is presented. Several tests are presented to demonstrate the performance of the ORMAS-PT method. © *2011 American Institute of Physics*. [doi:10.1063/1.3609756]

I. INTRODUCTION

The multi-configurational self-consistent field (MCSCF) approach is routinely used to treat chemical systems that exhibit near degeneracies and therefore require a multi-reference description.[1] Near degeneracies occur, for example, in the vicinity of conical intersections, during bond breaking, in free radical chemistry, electronic excited states, and unsaturated transition metal compounds. Every MCSCF wavefunction is expanded within a basis of configurations that are typically determined by a user-defined active space. An active space is comprised of a set of molecular orbitals (and electrons) that are needed to appropriately treat properties of interest. Each configuration corresponds to a unique distribution of electrons among the orbitals in the active space. It is common to employ a complete active space (CAS), which is a full configuration interaction (CI) computation within the active space. The CAS approach to MCSCF is known as the complete active space self-consistent field (CASSCF)[2] or the fully optimized reaction space (FORS)[3] method.

Although MCSCF provides qualitatively correct zeroth-order wavefunctions, the absence of dynamic correlation generally prevents quantitative agreement with experiment. Therefore, one needs to use the MCSCF wavefunction as a starting point for multi-reference configuration interaction (MRCI) or multi-reference perturbation theory (MRPT) calculations. Compared to MRCI, MRPT methods scale better with system size. To overcome the computational bottlenecks associated with MRCI, the Graphical Contracted Function (GCF) approach[4] shows promise. The Density Matrix Renormalization Group (DMRG) approach[5] also shows promise as a practical tool in the treatment of strongly correlated systems.[6] The present work is concerned with the MRPT methodology.

The conventional approach to n^{th} order perturbation theory considers the exact non-relativistic Hamiltonian as a perturbed independent particle (zeroth-order) Hamiltonian, with the energy and wavefunction expanded in n orders of perturbation.[7,8] In contrast to single reference perturbation theory, MRPT (including restricted open shell (ROHF) PT) is not uniquely defined. Consequently, there have been numerous MRPT methods developed.[9–12] Some of the most popular MRPT approaches are the complete active space second-order perturbation theory (CASPT2),[13] multi-state CASPT2 (MS-CASPT2),[14] multi-reference Møller-Plesset (MRMP) perturbation theory,[15] and multi-configurational quasi-degenerate perturbation theory (MCQDPT).[16] Both CASPT2/MS-CASPT2 and MRMP/MCQDPT employ a CAS reference wavefunction.

Over the past 15 years, developments in approximate CAS MRPT methods have facilitated the expansion of feasible CASSCF active spaces within the MRPT approach. Examples of such methods are the restricted active space perturbation theory through second order (RASPT2),[17,18] quasi-complete active space quasi-degenerate perturbation theory (QCASQDPT),[19] general MCQDPT (GMCQDPT),[20] and the reduced model space MRMP.[21] The reference wavefunctions for RASPT2 and QCASQDPT are the restricted active space self-consistent field (RASSCF)[22] and the quasi-complete active space (QCAS) type,[23] respectively.

The main difference between CAS MRPT and approximate CAS MRPT methods is that there are configurations that are normally present in the CAS but not in the approximate CAS reference space. These configurations, referred to here as IECs (internally excited configurations), can be significant,[20] and they should therefore be accounted for in the MRPT correction. The current implementation of RASPT2 does not consider the IECs,[17] while QCASQDPT and GMCQDPT do. However, the computational efficiency of the latter two methods suffers since the PT contributions are determined indirectly. That is, the reference configurations that couple to the excited configurations are not directly

a)Electronic mail:mark@si.msg.chem.iastate.edu.

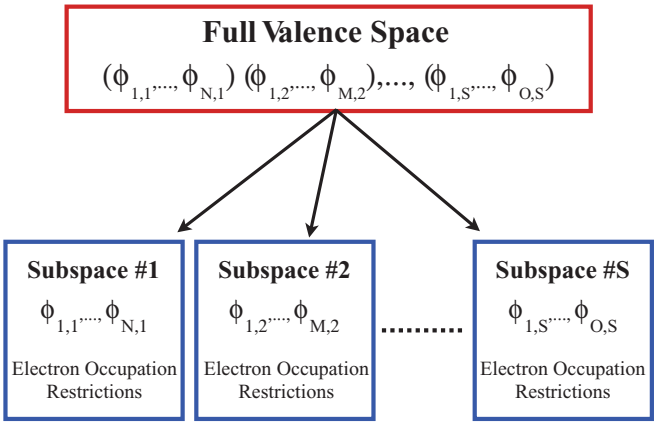

FIG. 1. Schematic representation of the ORMAS method. The full valence space orbitals are partitioned into S subspaces each containing N,M,...O orbitals, respectively. Minimum and maximum electron occupation restrictions are assigned to each subspace to determine which determinants from the original full valance space are used to construct the ORMAS Hamiltonian.

determined. It would therefore be beneficial to develop a general MRPT method that takes advantage of direct PT methodology and considers the IEC contributions to the MRPT properties.

The present paper introduces an alternative MRPT method that employs the occupation restricted multiple active space (ORMAS)[24] wavefunction as the zeroth order reference function. Similar to RASSCF and QCAS, the ORMAS method expands the wavefunction within a multi-electron basis that is typically much smaller than the corresponding CAS basis. The configurations included in the ORMAS expansion are specified through user-defined restrictions on the minimum and maximum electron occupation numbers for each user-defined orbital subspace (see Figure 1). Using ORMAS to appropriately partition a CAS, one can eliminate many ineffective electronic configurations ("*deadwood*"[25]) that contribute negligibly to the non-dynamic correlation. In this sense, the ORMAS approach has an analogous effect to that of the pre-screening of two-electron integrals. Thus, ORMAS has the ability to retain only the most important configurations in a CI space.

There are other methods that are similar to the ORMAS approach. Among these methods are the restricted configuration interaction (RCI) approach,[26] the generalized active space (GAS) method,[27] and the macroconfiguration approach.[28] ORMAS, RCI, GAS, and the macroconfiguration methods partition a set of active molecular orbitals into several subspaces (or groups) with restrictions imposed on the electron occupation numbers in each subspace. From the subspace specifications, a multi-electron basis is generated in which the wavefunction is expanded.

In comparison to RASPT2, ORMAS-PT provides greater flexibility within the reference wavefunction. ORMAS can generate a RASSCF wavefunction if desired, but it cannot generate a QCAS wavefunction. ORMAS does have the ability to generate a similar function (referred to as ORMAS0) that includes the QCAS reference determinants as a subset of the ORMAS0 CI expansion basis. Another feature of ORMAS is that the ORMAS wavefunction is expanded within a basis of determinants, thereby eliminating I/O by efficiently computing Hamiltonian matrix elements "on the fly" (direct CI). The direct CI methodology is adapted for the ORMAS-PT energy contributions described below.

II. THEORY

The ORMAS-PT method presented here follows the perturb-then-diagonalize prescription, based on the Hirao parallel direct determinant implementation[15,29,30] for FORS/CASSCF reference wavefunctions. As a consequence of the underlying ORMAS reference, there are distinct differences in how ORMAS-PT must be formulated compared to the MRMP/MCQDPT approach that is intended for a CAS reference. This section presents the Hirao MRPT procedure,[15] followed by a summary of the modifications that are required for ORMAS-PT.

In any PT method (single or multiple reference), the exact Hamiltonian (H) from the time-independent Schrödinger equation (Eq. (1)) is partitioned into a zeroth-order Hamiltonian (H_0) and a perturbation (V) (Eq. (2)).

$$H\Psi = E\Psi, \tag{1}$$

$$H = H_0 + V. \tag{2}$$

Hirao's MRMP approach defines H_0 as[15]

$$H_0 = \sum_c |\varphi_c\rangle\ \varepsilon_c\ \langle\varphi_c| + \sum_a |\varphi_a\rangle\ \varepsilon_a\ \langle\varphi_a| + \sum_e |\varphi_e\rangle\ \varepsilon_e\ \langle\varphi_e|\,. \tag{3}$$

In Eq. (3) φ_c, φ_a, and φ_e refer to the core-plus-inactive, active, and external molecular spin orbitals, respectively; ε_c, ε_a, and ε_e are the core-plus-inactive, active and external orbital energies, respectively. The orbital energies are defined as

$$\varepsilon_i = \langle\varphi_i\,|F|\,\varphi_i\rangle\,, \tag{4}$$

where F is the standard closed-shell Fock operator[31] given by

$$F_{ij} = h_{ij} + \sum_{kl} D^{\alpha}_{kl}\left[(ij\,|kl) - \tfrac{1}{2}(ik\,|jl)\right]. \tag{5}$$

In Eq. (5) i,j,k,l correspond to molecular spin orbitals, α denotes a particular MCSCF state, h_{ij} is an element of the one-electron Hamiltonian, (ij|kl) is an electron repulsion integral, and $\mathbf{D}^{\alpha}$ is the MCSCF one-particle density matrix for state α. The standard Fock operator is block diagonalized within the core-plus-inactive, the active, and the external orbital sub-blocks since the reference energy is invariant to orbital rotations within these orbital sub-blocks. Block diagonalization of **F** produces a set of canonical orbitals $\{\varphi\}$ and orbital energies $\{\varepsilon\}$ that are required in the MRPT expansion. This definition of H_0 (Eq. (3)) sets the zeroth-order energy for MCSCF state α to be the sum of the orbital energies $\{\varepsilon_i\}$ weighted by the corresponding diagonal elements of the one-particle density matrix D^{α}_{ii} (Eq. (6)).

$$E^{(0)}_{\alpha} = \left\langle\Psi^{(0)}_{\alpha}\right|H_0\left|\Psi^{(0)}_{\alpha}\right\rangle = \sum_i D^{\alpha}_{ii}\varepsilon_i. \tag{6}$$

A variety of correction functions can be incorporated into the MRMP H_0 in an attempt to improve the reliability of

MRPT; a summary of these is beyond the scope of the current work.[10] The present study is based on the "barycentric" definition of H_0 (Eq. (6)) used by Hirao[15] and is equivalent to the H_0 used in the Kozlowski-Davidson MROPT1 method.[10]

The scheme adopted here first performs the perturbation problem and then removes the degeneracy (if any) by solving the secular problem that corresponds to the effective Hamiltonian ($\mathbf{H}_{\text{eff}}$):

$$\left\langle \Psi_\alpha^{(0)} \middle| H_{\text{eff}} \middle| \Psi_\beta^{(0)} \right\rangle = E_\beta^{\text{MCSCF}} \delta_{\alpha\beta} + \frac{1}{2} \sum_{K}^{\text{SD(CAS)}} \times \left\{ \frac{\left\langle \Psi_\alpha^{(0)} \middle| H \middle| \Psi_K^{(0)} \right\rangle \left\langle \Psi_K^{(0)} \middle| H \middle| \Psi_\beta^{(0)} \right\rangle}{E_\beta^{(0)} - E_K^{(0)}} + \frac{\left\langle \Psi_\beta^{(0)} \middle| H \middle| \Psi_K^{(0)} \right\rangle \left\langle \Psi_K^{(0)} \middle| H \middle| \Psi_\alpha^{(0)} \right\rangle}{E_\alpha^{(0)} - E_K^{(0)}} \right\}. \quad (7)$$

In Eq. (7), MCSCF states are denoted by α and β, $\Psi_\alpha^{(0)}$ is the MCSCF reference wavefunction for state α, E_β^{MCSCF} is the MCSCF reference energy for state β, $E_\beta^{(0)}$ is the zeroth-order energy for state β (defined by Eq. (6)), $E_K^{(0)}$ is the zeroth-order energy (Eq. (6)) for a configuration K that is external to the MCSCF reference space, and the summation runs over all external configurations that do not differ by more than two spin orbitals from the reference configurations. For single state MRPT (MRMP), the effective Hamiltonian ($\mathbf{H}_{\text{eff}}$) is a 1×1 matrix, so the perturbative correction to that state is just the matrix itself. For more than one state, a multi-state MRPT requires the diagonalization of H_{eff} (MCQDPT).

Now consider a reformulation of the original Hirao MRPT method for the ORMAS-PT implementation. Modifications of the orbital canonicalization and the second order correction are necessary, whereas the definition of the zeroth-order Hamiltonian given above is retained (Eq. (3)).

To ensure that the ORMAS-PT energy is consistent regardless of how the reference wavefunction is constructed, the ORMAS-PT second-order energy correction is determined from a set of canonical orbitals that are obtained by block diagonalization of the standard Fock operator (Eq. (5)). The core-plus-inactive and external orbital sub-blocks are treated as previously described. Since the ORMAS reference energy is not invariant under orbital rotations *between* active subspaces, the active orbital sub-block of the Fock matrix itself is block diagonalized according to the user-defined orbital subspaces. For example, suppose an ORMAS active space is configured for three orbital subspaces. There would then be three active orbital sub-blocks in the standard Fock matrix, instead of a single active block as is used in a MRMP/MCQDPT treatment of a CAS reference.

In the limit of merging all ORMAS orbital subspaces, the second-order ORMAS-PT energy correction would be equivalent to the result obtained by the corresponding MRMP. Since a general ORMAS employs an incomplete active space, the second-order ORMAS-PT energy correction must be formulated to account for internally excited configurations (IECs). The IECs considered here correspond to single and double excitations from active orbitals to active orbitals such that the configurations that are created are not consistent with the ORMAS reference occupation restrictions on the orbital subspaces. IECs that correspond to triple and higher excitations from active molecular orbitals to active molecular orbitals are not considered. The general ORMAS-PT effective Hamiltonian is constructed according to Eq. (8).

$$\left\langle \Psi_\alpha^{(0)} \middle| H_{\text{eff}} \middle| \Psi_\beta^{(0)} \right\rangle = E_\beta^{\text{MCSCF}} \delta_{\alpha\beta} + \frac{1}{2} \sum_{K\notin \text{CAS}}^{\text{SD(ORMAS)}} \times \left\{ \frac{\left\langle \Psi_\alpha^{(0)} \middle| H \middle| \Psi_K^{(0)} \right\rangle \left\langle \Psi_K^{(0)} \middle| H \middle| \Psi_\beta^{(0)} \right\rangle}{E_\beta^{(0)} - E_K^{(0)}} + \frac{\left\langle \Psi_\beta^{(0)} \middle| H \middle| \Psi_K^{(0)} \right\rangle \left\langle \Psi_K^{(0)} \middle| H \middle| \Psi_\alpha^{(0)} \right\rangle}{E_\alpha^{(0)} - E_K^{(0)}} \right\} + \frac{1}{2} \sum_{K\notin \text{ORMAS}}^{\text{CAS}} \left\{ \frac{\left\langle \Psi_\alpha^{(0)} \middle| H \middle| \Psi_K^{(0)} \right\rangle \left\langle \Psi_K^{(0)} \middle| H \middle| \Psi_\beta^{(0)} \right\rangle}{E_\beta^{(0)} - E_K^{(0)}} + \frac{\left\langle \Psi_\beta^{(0)} \middle| H \middle| \Psi_K^{(0)} \right\rangle \left\langle \Psi_K^{(0)} \middle| H \middle| \Psi_\alpha^{(0)} \right\rangle}{E_\alpha^{(0)} - E_K^{(0)}} \right\}. \quad (8)$$

Similar to the MRMP/MCQDPT method, the MCSCF states are denoted by α and β. The first term on the right hand side (RHS) of Eq. (8) contributes the reference energy of MCSCF state β to the diagonal of the effective Hamiltonian. The first summation runs over all configurations K that are external to the CAS and do not differ by more than two spin-orbitals from the reference configurations. The second summation runs over all IECs. Neglecting the second summation on the RHS of Eq. (8) can potentially still provide satisfactory results,[17] but for a rigorous MRPT it is essential that this second summation be included. In implementing Eq. (8), the main challenge is to create an algorithm that enumerates the IECs and directly determines their contributions to $\mathbf{H}_{\text{eff}}$. This is discussed next.

The IECs are determined by initially relaxing the ORMAS reference restrictions on the minimum and maximum electron occupancies for each orbital subspace. Appropriately modifying the occupation restrictions provides criteria that the IECs must satisfy. Orbital subspace specifications permitting, these modifications allow each subspace to accommodate one or two additional electrons and to lose one or two electrons. The minimum and maximum orbital subspace occupation restrictions are modified as follows:

$$\bar{N}_I^{\max} = \begin{cases} N_I^{\max} + 2 & \text{if } \left(N_I^{\max} + 2\right) \le \text{number of orbitals in subspace I} \\ N_I^{\max} + 1 & \text{if } \left(N_I^{\max} + 1\right) = \text{number of orbitals in subspace I} \\ N_I^{\max} & \text{if } N_I^{\max} = \text{number of orbitals in subspace I} \end{cases} \quad \text{For I} = 1, \text{X}, \quad (9)$$

$$\bar{N}_I^{min} = \begin{cases} N_I^{min} - 2 & \text{if } \left(N_I^{min} - 2\right) \geq 2 \\ N_I^{min} - 1 & \text{if } N_I^{min} = 1 \\ N_I^{min} & \text{if } N_I^{min} = 0 \end{cases} \quad \text{For I} = 1, \text{X}. \tag{10}$$

In Eqs. (9)–(10), X is the number of ORMAS orbital subspaces, $N_I^{min}(N_I^{max})$ specifies the reference occupation restrictions on the minimum (maximum) electron occupations for subspace I, and $\bar{N}_I^{min}(\bar{N}_I^{max})$ is the modified minimum (maximum) electron occupation restriction for subspace I.

Modified occupation restrictions are used to generate α-groups and β-groups, which describe the distribution of the α-electrons and β-electrons among the X ORMAS orbital subspaces. These α-groups and β-groups are then combined in a pair-wise procedure to find combinations that adhere to the modified electron occupation restrictions. For each valid combination, α-strings and β-strings are enumerated[24] from the α-group and β-group, respectively. These α-strings and β-strings are combined to form determinants; the α-strings and β-strings indicate which α and β molecular spin-orbitals are occupied. The resulting determinants correspond not only to the IECs, but also to the reference determinants.

It is necessary to categorize each IEC specifically, because a single algorithm cannot directly determine the energy contributions for all IECs. This is analogous to the need for separate treatments of determinants that correspond to valence-to-external vs. active-to-external electronic excitations, as is required in MRMP/MCQDPT formulations. The scheme introduced here classifies each IEC into one of eight types; these types are listed in Table I and are discussed in detail in the following paragraphs.

Each IEC classification is based upon how the electron occupations in each orbital subspace are not consistent with the minimum and maximum electron occupation restrictions of the reference specifications (N_I^{min} and N_I^{max}; for I = 1, X). With respect to reference occupation restrictions, an inconsistency would correspond to a subspace being 'over-occupied' (too many electrons) or 'under-occupied' (too few electrons). For example, if $N_I^{max} = 4$ for subspace I and subspace I actually contains five electrons, then subspace I is 'over-occupied' by one electron.

The symbol $R_I^{P,Q}$ is introduced here to monitor whether subspace I is consistent with the reference occupation restrictions when α-group P is combined with β-group Q. In Eq. (11) below, $N_{I,P}^{\alpha}$ ($N_{I,Q}^{\beta}$) is the number of α-electrons (β-electrons) assigned to subspace I from α-group P (β-group Q), N_I^{min} and N_I^{max} (defined above) are the minimum and maximum occupation restrictions for reference subspace I. An 'under-occupied' ('over-occupied') subspace corresponds to $R_I^{P,Q} < 0$ ($R_I^{P,Q} > 0$) while $R_I^{P,Q} = 0$ indicates subspace I is consistent with the reference occupation restrictions. For example, $R_I^{P,Q} = -2$ indicates subspace I is 'under-occupied' by two electrons.

$$R_I^{P,Q} = \begin{cases} \left(N_{I,P}^{\alpha} + N_{I,Q}^{\beta} - N_I^{min}\right) & \text{if } \left(N_{I,P}^{\alpha} + N_{I,Q}^{\beta} - N_I^{min}\right) < 0 \\ \left(N_{I,P}^{\alpha} + N_{I,Q}^{\beta} - N_I^{max}\right) & \text{if } \left(N_{I,P}^{\alpha} + N_{I,Q}^{\beta} - N_I^{max}\right) > 0 \\ 0 & \text{otherwise} \end{cases} \quad \text{For I} = 1, \text{X}. \tag{11}$$

$R_I^{P,Q}$ can be used to compute a label, $\Delta_{P,Q}$ (employing Eqs. (12)–(15) below) that classifies a set of IECs that are generated from the combination of α-group P with β-group Q.

$$Y_{P,Q} = \sum_I^X R_I^{P,Q}, \tag{12}$$

$$Z_{P,Q} = \sum_I^X \left|R_I^{P,Q}\right|, \tag{13}$$

$$\gamma_{P,Q} = \begin{cases} 1 & \text{if } Y_{P,Q} \geq 1 \\ -1 & \text{if } Y_{P,Q} < 1, \end{cases} \tag{14}$$

$$\Delta_{P,Q} = \gamma_{P,Q}(|Y_{P,Q}| + 2^{Z_{P,Q}}). \tag{15}$$

In Eqs. (12)–(15), $Y_{P,Q}$ is a sum over all 'under-occupations' and 'over-occupations' ($R_I^{P,Q}$) for each subspace, $Z_{P,Q}$ is an *absolute* sum over all 'under-occupations' and 'over-occupations' for each subspace, $\gamma_{P,Q}$ is a sign transfer function, and $\Delta_{P,Q}$ is the resulting IEC label. All IEC labels are calculated on the fly since their storage requirements can be excessive.

The first column in Table I lists all possible $\Delta_{P,Q}$ labels (IEC types). Regardless of the how the ORMAS wavefunction is constructed, only eight unique values of $\Delta_{P,Q}$ correspond to single or double IECs. The value $\Delta_{P,Q} = 1$ corresponds to the reference configurations. Each of these values is described next. Unless indicated otherwise, all subspaces are consistent with the reference occupation restrictions.

TABLE I. Classification types of internally excited configurations (IEC). IEC type corresponds to how the subspaces have too many (positive integer) or too few (negative integer) electrons with respect to the ORMAS reference specifications. $R_I^{P,Q}$ indicates how subspace I is "under-occupied"/"over-occupied" upon combining α-group P with β-group Q (a zero integer means there is no violation in that subspace). $\Delta_{P,Q} = 1$ corresponds to IECs that are reference determinants.

	Electron "over-occupations"/"under-occupations" in subspace:						
IEC type $\Delta_{P,Q}$	$R_1^{P,Q}$	$R_2^{P,Q}$	$R_3^{P,Q}$	$R_4^{P,Q}$	$R_5^{P,Q}$	$R_6^{P,Q} \ldots R_{N-1}^{P,Q}$	$R_N^{P,Q}$
1[a]	0	0	0	0	0	0…0	0
−3	–1	0	0	0	0	0…0	0
3	1	0	0	0	0	0…0	0
4	1	−1	0	0	0	0…0	0
−6	–2	0	0	0	0	0…0	0
−6	–1	−1	0	0	0	0…0	0
6	2	0	0	0	0	0…0	0
6	1	1	0	0	0	0…0	0
−9	–2	1	0	0	0	0…0	0
−9	–1	−1	1	0	0	0…0	0
9	–1	2	0	0	0	0…0	0
9	–1	1	1	0	0	0…0	0
16	–2	2	0	0	0	0…0	0
16	–2	1	1	0	0	0…0	0
16	–1	−1	2	0	0	0…0	0
16	–1	−1	1	1	0	0…0	0

[a] $\Delta_{P,Q} = 1$ corresponds to determinants that are part of the ORMAS reference space.

$\Delta_{P,Q} = 1$: all subspaces adhere to reference occupation restrictions (not excited configurations)

$\Delta_{P,Q} = -3$: one subspace is 'under-occupied' by one electron.

$\Delta_{P,Q} = 3$: one subspace is 'over-occupied' by one electron.

$\Delta_{P,Q} = 4$: one subspace is 'over-occupied' by one electron *and* one other subspace is 'under-occupied' by one electron.

$\Delta_{P,Q} = -6$: *either* one subspace is 'under-occupied' by two electrons *or* two subspaces are both 'under-occupied' by one electron.

$\Delta_{P,Q} = 6$: *either* one subspace is 'over-occupied' by two electrons *or* two subspaces are both 'over-occupied' by one electron.

$\Delta_{P,Q} = -9$: one subspace is 'over-occupied' by one electron *and either* one other subspace is 'under-occupied' by two electrons *or* two other subspaces are both 'under-occupied' by one electron

$\Delta_{P,Q} = 9$: one subspace is 'under-occupied' by one electron *and either* one other subspace is 'over-occupied' by two electrons *or* two other subspaces are both 'over-occupied' by one electron.

$\Delta_{P,Q} = 16$: (four situations are possible)

(1) one subspace is 'under-occupied' by two electrons *and* one other subspace in 'over-occupied' by two electrons.
(2) one subspace is 'under-occupied' by two electrons *and* two other subspaces are both 'over-occupied' by one electron.
(3) two subspaces are both 'under-occupied' by one electron *and* one other subspace is 'over-occupied' by two electrons.
(4) two subspaces are both 'under-occupied' by one electron *and* two other subspaces are both 'over-occupied' by one electron.

As illustrated in Table I, the different cases for a given $\Delta_{P,Q}$ are distinguished by the corresponding values of $R_I^{P,Q}$. Configurations that have $\Delta_{P,Q} = 1$ are reference configurations and are not included in the summation over the IEC (second summation in Eq. (8)). In addition, some α-group and β-group combinations can correspond to triple and higher excited determinants. These IECs cannot couple with any of the reference configurations and are also not considered in the ORMAS-PT.

From each α-group/β-group pair corresponding to an IEC label that characterizes a single or double excitation, α-strings and β-strings are enumerated and combined pair-wise to form the proper IECs. These IECs are treated with the appropriate algorithm that corresponds to their $\Delta_{P,Q}$ labels. This classification scheme allows for a highly efficient algorithm that directly computes the ORMAS-PT energy contributions.

To illustrate the above scheme, consider employing ORMAS to partition a singlet system of 6 electrons and 12 orbitals into three 4-orbital subspaces. The minimum (maximum) reference occupation restrictions for the three orbital subspaces are set to 0,0,0 (6,6,6). Thus, any distribution of electrons among the subspaces is allowed. There are 28 possible distributions of the 6 electrons (seen in Table II); the total number of electrons in subspace I for distribution J is indicated by $N_{I,J}$. These 28 distributions correspond to a total of 48,400 determinants. This is identical to a full CAS, so the IECs are not relevant in this case.

Next, consider the minimum (maximum) reference occupation restrictions for each subspace to be 2,2,2 (2,2,2).

TABLE II. All possible distributions of 6 electrons among the three four-orbital subspaces. Distribution 13 is the only allowable distribution of electrons with the minimum (maximum) electron occupation restrictions of 2 (2) for each subspace. $N_{I,J}$ indicates the number of electrons assigned to subspace I from distribution J.

Distribution (J)	$N_{1,J}$	$N_{2,J}$	$N_{3,J}$	# Determinants
1	6	0	0	16
2	5	1	0	192
3	5	0	1	192
4	4	2	0	768
5	4	1	1	1664
6	4	0	2	768
7	3	3	0	1184
8	3	2	1	4416
9	3	1	2	4416
10	3	0	3	1184
11	2	4	0	768
12	2	3	1	4416
13	**2**	**2**	**2**	**7552**
14	2	1	3	4416
15	2	0	4	768
16	1	5	0	192
17	1	4	1	1664
18	1	3	2	4416
19	1	2	3	4416
20	1	1	4	1664
21	1	0	5	192
22	0	6	0	16
23	0	5	1	192
24	0	4	2	768
25	0	3	3	1184
26	0	2	4	768
27	0	1	5	192
28	0	0	6	16

These restrictions allow for just a single distribution (distribution 13) while all other distributions correspond to IECs (distributions 1–12, 14–28). Not all of the distributions that correspond to IECs will contribute to the ORMAS-PT energy. For example consider distribution 2 in Table II: subspace one is 'over-occupied' by three electrons, subspace two is 'under-occupied' by one electron, and subspace three is 'under-occupied' by two electrons. IECs corresponding to distribution 2 represent triple excitations since subspace one is 'over-occupied' by three electrons. IECs corresponding to triple excitations cannot couple to determinants in the ORMAS reference space, so these IECs will not contribute to the ORMAS-PT energy. On the other hand, consider distribution 4 in Table II: subspace one is 'over-occupied' by two electrons, subspace two is consistent with the reference occupation restriction, and subspace three is 'under-occupied' by two electrons. Therefore, IECs from distribution 4 correspond to double excitations from the ORMAS reference space. Because of this, IECs corresponding to distribution 4 will make contributions to the wavefunction and energy. The numerical IEC label given to any α-group P and β-group Q combination that results in the distribution 4 is $\Delta_{P,Q} = 16$ (see Eqs. (11)–(15) and Table I).

An appropriate $\Delta_{P,Q}$ label is assigned for each α-group P/β-group Q pair. Once $\Delta_{P,Q}$ for a particular pair is known, the appropriate algorithm can be executed to directly determine the IEC contributions to the energy and wavefunction. The above prescription is also applied to the excited configurations that are external to the CAS (the first summation on the RHS of Eq. (8)). These external terms require the greatest amount of computational effort.

III. APPLICATIONS

The ORMAS-PT method has been implemented in the GAMESS (General Atomic and Molecular Electronic Structure System)[32] suite of programs. GAMESS has been used for all calculations that are presented here. The ORMAS-PT method is benchmarked against full MRMP/MCQDPT results for four test cases, including a state averaged MCSCF wavefunction, singlet and higher spin states, and ionic systems.

A. Potential energy surface of lithium fluoride

The LiF dissociation energy curves for the two lowest energy $^1\Sigma^+$ states at the equilibrium LiF ground state geometry are examined to determine whether ORMAS-PT can properly account for the avoided crossing between these two surfaces. Near the LiF equilibrium geometry, the lower energy $^1\Sigma^+$ state may be described as ionic, or at least highly polar, while the higher energy state may be described as covalent. After the avoided crossing the lower $^1\Sigma^+$ state becomes covalent, while the higher energy $^1\Sigma^+$ state is ionic. In C_{2v} symmetry, the reference CAS wavefunction is constructed from six electrons and nine active orbitals CAS(6,9): $4a_1$,$5a_1$,$6a_1$,$1b_1$,$2b_1$,$3b_1$,$1b_2$,$2b_2$,$3b_2$. Molecular orbitals $1a_1$, $2a_1$, and $3a_1$ correspond to the fluorine 1s and 2s and lithium 1s atomic orbitals. These orbitals are chemically inactive and remain in the core.

Using ORMAS, the CAS(6,9) space is partitioned into three 3-orbital subspaces: {$4a_1$, $5a_1$, $6a_1$}, {$1b_1$, $2b_1$, $3b_1$}, and {$1b_2$, $2b_2$, $3b_2$}. The electron occupation restrictions for each orbital subspace are set to a minimum (maximum) of 2 (2) electrons. These occupation restrictions permit only two electrons to occupy any of the subspaces, irrespective of spin. The 6-311++G(3df,3pd)[33] basis set is used for all MCQDPT and ORMAS-PT calculations. The orbitals are state-averaged over the two lowest energy $^1\Sigma^+$ states.

Figure 2 shows the two lowest $^1\Sigma^+$ potential energy curves for ORMAS-PT and MCQDPT. Note that in Figure 2 that there are actually four curves but the ORMAS-PT and MCQDPT curves overlap making it difficult to distinguish between the two. Additionally, ORMAS-PT is able to account for the qualitative features of the two surfaces, namely the equilibrium geometry and the avoided crossing around 12-13 bohr. Figure 3 shows the relative error of the singlet-singlet ORMAS-PT energy splitting relative to the MCQDPT values. Beyond 2.9 bohr ($r_{eq} = 2.98$ bohrs)[34] there is less than 0.2 kcal/mol error between ORMAS-PT and MCQDPT. At shorter distances ORMAS-PT overestimates the energy splitting by up to 3 kcal/mol. The large error [2.4 and

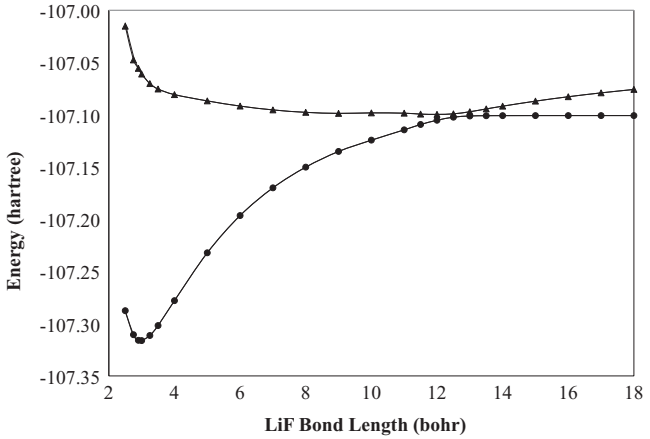

FIG. 2. Potential energy curve (hartree) for the dissociation of LiF. The ● and ▲ designate the two lowest $^1\Sigma^+$ states.

3.0 kcal/mol] in the singlet-singlet energy splitting at the two shortest bond distances may arise because ORMAS does not give an adequate reference wavefunction for both $^1\Sigma^+$ states, and this carries over to the ORMAS-PT results. For increased accuracy, the ORMAS molecular orbital subspace restrictions should be relaxed to generate a more reliable reference wavefunction.

B. Potential energy surface of $Si_{15}H_{16}$ dimer buckling modes

Whether or not Si(100) ground state surface dimers are buckled is an unresolved matter since highly correlated methods are impractical for the large surface models needed to eliminate edge effects. To circumvent the computational expense of large cluster models, small surface clusters are routinely used (Figure 4(a)). To investigate the geometry of the Si(100) surface dimers on the MRPT ground state PES, one can first calculate the MCSCF vibrational modes that correspond to the buckling frequencies. The geometries are then perturbed along these modes while calculating MRPT single point energies.

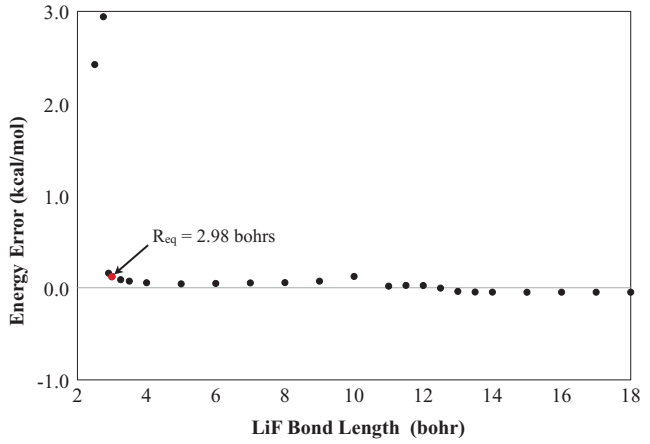

FIG. 3. ORMAS-PT relative error (kcal/mol) for the energy splitting for the two lowest $^1\Sigma^+$ states compared to MCQDPT.

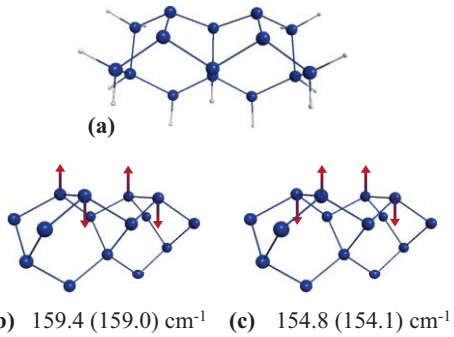

FIG. 4. (A) Optimized structure of $Si_{15}H_{16}$. (B) buckling mode-1, (C) buckling mode-2. For clarity, the hydrogen atoms in B and C been removed. The buckling mode frequencies in B and C correspond to those calculated with CASSCF and ORMAS(in parentheses).

At both the FORS/CASSCF and ORMAS-SCF levels of theory, the cc-pVDZ basis set[35] was used to optimize $Si_{15}H_{16}$. Subsequently, the Hessian (matrix of second order energy derivatives) was diagonalized to determine the vibrational modes. Geometric distortions along two buckling modes of $Si_{15}H_{16}$ were then performed. The CASSCF active space includes one σ/σ^* and one π/π^* pair from each dimer, leading to a total of 8 electrons distributed among 8 molecular orbitals (8,8).

For ORMAS-SCF, each dimer is given its own subspace. This results in two subspaces, each containing four molecular orbitals (one σ/σ^* and one π/π^* pair). The reference occupation restrictions for the ORMAS-SCF subspaces are set to a minimum (maximum) of 4 (4) electrons. The FORS/CASSCF and ORMAS-SCF buckling vibration modes for $Si_{15}H_{16}$ may be seen in Figure 4. The hydrogen atoms are eliminated for clarity in Figures 4(b) and 4(c). The two buckling modes are referred to as mode-1 and mode-2.

As seen in Figure 5, displacements along the two buckling modes show that the ORMAS-PT surface features agree nicely with the MRMP result that the MRPT energy increases as the atoms are displaced along the buckling modes. The absolute errors in mode-1 and mode-2 between the two

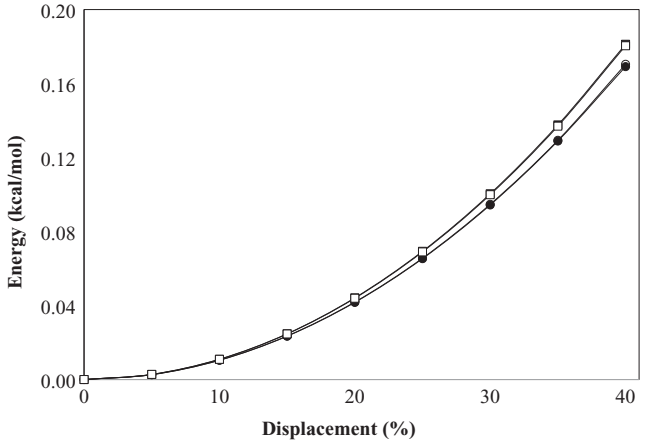

FIG. 5. MRPT potential energy curves (kcal/mol) for the displacement $Si_{15}H_{16}$ from the optimized geometries of FORS/CASSCF and ORMAS along buckling mode 1 (●, ◯) and mode 2 (▮, □). The filled markers refer to the MRMP energy while the unfilled markers refer to ORMAS-PT.

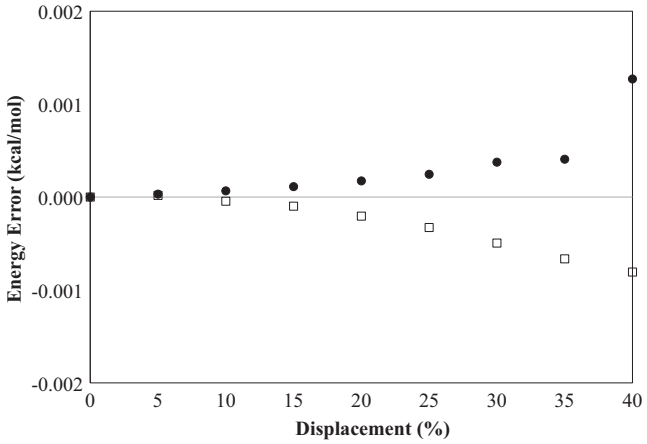

FIG. 6. Relative mode 1 (●) and mode 2 (□) errors (kcal/mol) with respect to the minimum energy structure for ORMAS-PT compared to MRMP.

methods are negligible (Figure 6). The energy error (kcal/mol) is small, even though the displaced geometries are slightly different, since the structures are perturbed along modes that correspond to an ORMAS-SCF vs. a FORS/CASSCF reference. This good agreement attests to the reliability of a properly constructed ORMAS wavefunction, and that ORMAS-PT is suitable for predicting MRMP energy differences.

C. Singlet-triplet and doublet-quartet splitting of OxoMn(salen) and OxoMn(salen)$^{-1}$

The catalyst chloro-4,4'-(1,2-ethanediyldinitrilo)bis(2-pentanonato)(2-)N,N',O,O')-m-oxomanganese, referred to here as oxoMn(salen) (Figure 7), has been previously studied[36] using the CAS MRPT method, but is reexamined here to determine the suitability of ORMAS-PT for transition metal complexes. Geometry optimizations on the singlet (neutral) and the doublet and quartet (ionic) species were performed using the 6-31G(d) basis set.[37] The triplet MCSCF state spontaneously dissociates the oxygen atom upon optimization from the bound singlet geometry.[38] Consequently, triplet calculations presented here were done at the corresponding optimized singlet geometries. In addition, ORMAS-PT singlet-triplet splittings were computed at both the CASSCF and ORMAS optimized geometries. ORMAS-PT doublet-quartet splittings were computed at the ORMAS optimized geometries only.

Three different active spaces are employed to treat the singlet and triplet spin states for oxoMn(salen).

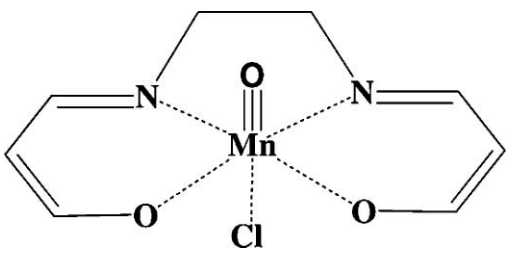

FIG. 7. OxoMn(salen).

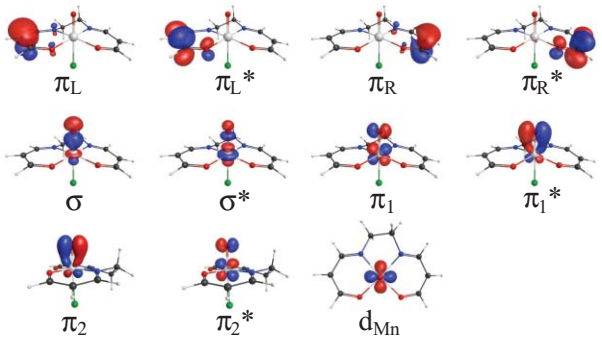

FIG. 8. OxoMn(salen) CASSCF/6-31G(d) MCSCF optimized orbitals.

The first active space corresponds to a CAS with 12 electrons distributed among the 11 active orbitals depicted in Figure 8. The second active space (ORMAS-3) partitions the active orbitals into three subspaces: $\{\pi_L\pi_L^*\}$,$\{\pi_R\pi_R^*\}$, and $\{\pi_1\pi_1^*\pi_2\pi_2^*\sigma\sigma^*d_{MN}\}$ with electron occupations restricted to a minimum (maximum) of 2,2,8 (2,2,8), respectively. The final active space (ORMAS-6) partitions the active orbitals into six subspaces: $\{\pi_L\pi_L^*\}$,$\{\pi_R\pi_R^*\}$,$\{\pi_1\pi_1^*\}$,$\{\pi_2\pi_2^*\}$,$\{\sigma\sigma^*\}$, and $\{d_{MN}\}$ with electron occupations restricted to a minimum (maximum) of 2,2,2,2,2,1 (2,2,4,4,4,2), respectively.

There are only slight modifications to two of the active subspaces for the anionic doublet and quartet states of oxoMn(salen)$^{-1}$. Here the FORS/CASSCF active space is specified to have 13 electrons distributed among the same 11 active orbitals (13,11). For ORMAS, the subspace orbitals for the anionic species are partitioned in the same way as in the neutral species. The difference between the neutral and anionic specifications concerns the electron occupation restrictions. The electron occupation restrictions for the ORMAS-3 orbital subspaces are set to a minimum and maximum of 2,2,9 (2,2,9), while the ORMAS-6 orbital subspace restrictions are the same as those used for the neutral species.

Table III shows the singlet-triplet energy splitting of neutral oxoMn(salen) for the three selected active spaces. Using the CAS MRPT energy as the benchmark, the ORMAS-3 active space is in the best agreement for the predicted singlet-triplet splitting. If one uses the CAS geometry to calculate the ORMAS-3 PT singlet-triplet splitting, the ORMAS-3 PT error is ~1.8 kcal/mol. However, when the geometry is optimized with ORMAS-3, the ORMAS-3 PT error decreases to only ~0.1 kcal/mol. The ORMAS-6 PT predicted singlet-triplet splitting is in error by ~2.5 kcal/mol at the CASSCF geometry and by ~2.6 kcal/mol at the ORMAS-6 geometry. The ORMAS-6 and ORMAS-6//CAS PT prediction that the singlet state lies lower in energy than the triplet state is incorrect. Since the singlet-triplet splitting is small, this error may imply that a more compete active space is needed.

For the oxoMn(salen)$^{-1}$ anion, the doublet-quartet splitting (Table IV) is calculated to be much larger than the singlet-triplet splitting in the neutral species. For the anion, both the ORMAS-3 PT and ORMAS-6 PT predicted splittings agree with CAS MRPT to within ~0.6 kcal/mol. The good agreement between both the neutral and anionic oxoMn(salen)

TABLE III. MCSCF and MRPT singlet-triplet energy splitting for oxoMn(salen) using a complete active space and two different ORMAS partitions.

System	Method	Active Space	MCSCF Singlet-Triplet Splitting (kcal/mol)	MRPT Singlet-Triplet Splitting (kcal/mol)	# of Determinants	Time for PT correction (min)[a]
^{1}A oxoMn (salen)	CAS	(12,11)	–	–	213,444	209
	ORMAS-3[b]//CAS[c]	$\{d_{Mn},\sigma,\sigma^*,\pi_1,\pi_1^*,\pi_2,\pi_2^*\}$, $\{\pi_L,\pi_L^*\},\{\pi_R,\pi_R^*\}$	–	–	34,104	42
	ORMAS-6[d]//CAS[c]	$\{d_{Mn}\},\{\sigma,\sigma^*\},\{\pi_1,\pi_1^*\}$, $\{\pi_2,\pi_2^*\},\{\pi_L,\pi_L^*\},\{\pi_R,\pi_R^*\}$	–	–	11,520	16
	ORMAS-3[b]	$\{d_{Mn},\sigma,\sigma^*,\pi_1,\pi_1^*,\pi_2,\pi_2^*\}$, $\{\pi_L,\pi_L^*\},\{\pi_R,\pi_R^*\}$	–	–	34,104	42
	ORMAS-6[d]	$\{d_{Mn}\},\{\sigma,\sigma^*\},\{\pi_1,\pi_1^*\}$, $\{\pi_2,\pi_2^*\},\{\pi_L,\pi_L^*\},\{\pi_R,\pi_R^*\}$	–	–	11,520	16
^{3}A oxoMn (salen)	CAS	(12,11)	−0.3	−2.2	152,460	293
	ORMAS-3[b]//CAS[c]	$\{d_{Mn},\sigma,\sigma^*,\pi_1,\pi_1^*,\pi_2,\pi_2^*\}$, $\{\pi_L,\pi_L^*\},\{\pi_R,\pi_R^*\}$	−0.3	−0.4	24,948	51
	ORMAS-6[d]//CAS[c]	$\{d_{Mn}\},\{\sigma,\sigma^*\},\{\pi_1,\pi_1^*\}$, $\{\pi_2,\pi_2^*\},\{\pi_L,\pi_L^*\},\{\pi_R,\pi_R^*\}$	−1.3	0.3	8,742	19
	ORMAS-3[b]	$\{d_{Mn},\sigma,\sigma^*,\pi_1,\pi_1^*,\pi_2,\pi_2^*\}$, $\{\pi_L,\pi_L^*\},\{\pi_R,\pi_R^*\}$	−0.2	−2.3	24,948	51
	ORMAS-6[d]	$\{d_{Mn}\},\{\sigma,\sigma^*\},\{\pi_1,\pi_1^*\}$, $\{\pi_2,\pi_2^*\},\{\pi_L,\pi_L^*\},\{\pi_R,\pi_R^*\}$	−1.0	0.4	8,742	19

[a]Total time for computing PT energy correction on two dual-quad core Intel Xeon R5420 nodes.
[b]Minimum(maximum) electron occupation restrictions respective to active space: 8,2,2(8,2,2).
[c]ORMAS calculation performed at the singlet CAS optimized geometry.
[d]Minimum(maximum) electron occupation restrictions respective to active space: 1,2,2,2,2,2(2,4,4,4,2,2).

species demonstrates the ability of ORMAS to provide a reliable reference wavefunction for the MRPT correction.

For both the neutral and anionic oxoMn(salen) species, going from the full CAS MRPT treatment to ORMAS-3 (or ORMAS-6) decreases both the number of determinants and CPU time[39] (Tables III and IV) significantly. For the open shell systems, ORMAS-PT uses ∼1–2 orders of magnitude fewer determinants and ∼1 order of magnitude less CPU time compared to CAS MRPT. The ability to use fewer determinants through an ORMAS wavefunction decreases the CPU time, and more importantly the system memory requirements also decrease.

D. Trans-polyacetylene ionization potentials

ORMAS-PT vertical ionization potentials (IPs) for several *trans*-polyacetylene polymers are now examined to understand the convergence of ORMAS-PT predicted IPs to MRMP results. The IP is calculated from the difference in absolute energies of the neutral and ionized species for systems comprised of 2–8 ethylene subunits (Figure 9). The energies of the ionized species are calculated at the optimized geometries of the corresponding neutral species. These systems are highly conjugated, so the active space is constructed around the π orbitals and π electrons.

TABLE IV. MCSCF and MRPT doublet-quartet energy splitting for oxoMn(salen)$^{-1}$ using a complete active space and two different ORMAS partitions.

System	Method	Active Space	MCSCF Doublet-Quartet Splitting (kcal/mol)	MRPT Doublet-Quartet Splitting (kcal/mol)	# of Determinants	Time for PT correction (min)[a]
^{2}A oxoMn(salen)$^{-1}$	CAS	(13,11)	–	–	152,460	313
	ORMAS-3[b]	$\{d_{Mn},\sigma,\sigma^*,\pi_1,\pi_1^*,\pi_2,\pi_2^*\}$, $\{\pi_L,\pi_L^*\},\{\pi_R,\pi_R^*\}$	–	–	21,336	47
	ORMAS-6[c]	$\{d_{Mn}\},\{\sigma,\sigma^*\},\{\pi_1,\pi_1^*\}$, $\{\pi_2,\pi_2^*\},\{\pi_L,\pi_L^*\},\{\pi_R,\pi_R^*\}$	–	–	12,582	28
^{4}A oxoMn(salen)$^{-1}$	CAS	(13,11)	−6.9	−10.8	76,230	157
	ORMAS-3[b]	$\{d_{Mn},\sigma,\sigma^*,\pi_1,\pi_1^*,\pi_2,\pi_2^*\}$, $\{\pi_L,\pi_L^*\},\{\pi_R,\pi_R^*\}$	−6.7	−10.2	11,193	25
	ORMAS-6[c]	$\{d_{Mn}\},\{\sigma,\sigma^*\},\{\pi_1,\pi_1^*\}$, $\{\pi_2,\pi_2^*\},\{\pi_L,\pi_L^*\},\{\pi_R,\pi_R^*\}$	−7.9	−10.4	6,972	16

[a]Total time for computing PT energy correction on two dual-quad core Intel Xeon R5420 nodes.
[b]Minimum(maximum) electron occupation restrictions respective to active space: 9,2,2(9,2,2).
[c]Minimum(maximum) electron occupation restrictions respective to active space: 1,2,2,2,2,2(2,4,4,4,2,2).

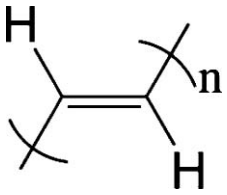

FIG. 9. Schematic of *trans*-polyacetylene of length n.

The MRMP calculations use a CAS reference wavefunction that corresponds to an active space of size (2n,2n), where n is the number of ethylene subunits. For the ORMAS-PT IPs, the active molecular orbitals are partitioned into two orbital subspaces. With respect to the RHF determinant, the first subspace (space 1) corresponds to the occupied π molecular orbitals while the unoccupied π^* molecular orbitals comprise the second subspace (space 2). A maximum of two, three, or four electrons are allowed to excite from orbitals in space 1 to orbitals in space 2. The minimum (maximum) reference occupation restrictions for space 1 and space 2 are set to 2n-MAX and 0 (2n and MAX), where MAX = 2,3,4 depending on the level of excitation. All calculations use the cc-pVTZ basis set.[35]

Table V shows ORMAS-SCF and CASSCF IPs for *trans*-polyacetylene polymers of length n. For polymers of length n = 3–8, the ORMAS-SCF IPs oscillate slightly from MAX = 2 to 3 to 4, but these variations are very small. At the highest excitation level (MAX = 4) there is good agreement between the ORMAS-SCF and CASSCF (maximum error ~0.02 eV). Both ORMAS-SCF and CASSCF under-estimate vertical IPs compared with the experimental values for polymers of length n = 2,3,4.[40] It is therefore likely that the ORMAS-SCF and CASSCF IPs are also underestimated for the longer polymers (n = 5–8).

Table VI shows ORMAS-PT and MRMP IPs for *trans*-polyacetylene polymers of length n. The MRMP IPs for polymers of length n = 2,3,4 are in agreement with experiment. From this it is clear that dynamic correlation is important to reliably predict IPs for *trans*-polyacetylene polymers. For polymer n = 3, the progression from MAX = 2,3,4 shows that the ORMAS-PT errors increase as MAX increases. For polymers of length n = 4–8, the ORMAS-PT predicted vertical IPs exhibit good convergence to the MRMP values. The error for these longer polymers range from 0.08–0.11 eV, 0.04–0.8 eV, and 0.01–0.05 eV for excitation levels set to MAX = 2, MAX = 3, and MAX = 4, respectively. ORMAS-PT is an efficient alternative to MRMP, as it uses 1–2 orders of magnitude fewer determinants. For *trans*-polyactylene polymers of length n = 8 (or larger), ORMAS-PT is an efficient approach to compute the IPs.

TABLE V. MCSCF ionization potentials (eV) and experimental ionization potentials for polyethylene polymers of length n subunits.

Ethylene subunits	CAS size	ORMAS-SCF Max = 2	ORMAS-SCF Max = 3	ORMAS-SCF Max = 4	CASSCF	Exp.
2	(4,4)	8.38	–	–	8.47	9.09
3	(6,6)	7.71	7.72	7.78	7.78	8.29–8.45
4	(8,8)	7.27	7.22	7.34	7.35	7.8-8.1
5	(10,10)	6.97	6.89	7.06	7.07	–
6	(12,12)	6.77	6.66	6.86	6.87	–
7	(14,14)	6.62	6.48	6.71	6.73	–
8	(16,16)	6.51	6.35	6.60	–	–

TABLE VI. MRPT ionization potentials (eV) and experimental ionization potentials for polyethylene polymers of length n subunits.

Ethylene subunits	CAS size	ORMAS-PT Max = 2	ORMAS-PT Max = 3	ORMAS-PT Max = 4	MRMP	Exp.
2	(4,4)	9.23	–	–	9.11	9.09
3	(6,6)	8.32	8.59	8.62	8.34	8.29–8.45
4	(8,8)	7.92	7.66	7.86	7.88	7.8–8.1
5	(10,10)	7.65	7.63	7.57	7.58	–
6	(12,12)	7.50	7.47	7.35	7.39	–
7	(14,14)	7.41	7.36	7.22	7.27	–
8	(16,16)	7.37	7.30	7.13	–	–

IV. CONCLUSIONS

A quasi-degenerate perturbation theory based on the ORMAS reference wavefunction has been described. For a complete active space MRPT, the effective Hamiltonian considers singly and doubly excited configurations, into the external orbital space of the MCSCF. For ORMAS-PT, the effective Hamiltonian was reformulated to also include internally excited configurations (IECs). A scheme was presented that determines the IECs and allows for a direct computation of the IEC contributions to the ORMAS-PT energy and wavefunction. This same scheme can be applied to the excited configurations outside of the complete active space (CAS) to increase the efficiency of ORMAS-PT method.

The ORMAS-PT method has been applied to four different systems, with the following key conclusions:

(1) For the two lowest $^1\Sigma^+$ states of LiF, ORMAS-PT reproduces the MCQDPT avoided crossing between the two state-averaged potential energy surfaces. The energy splitting between the two states shows the largest error for LiF bond lengths less than the equilibrium distance. Starting from the LiF equilibrium bond distance and longer, the error in the energy splitting is less than 0.2 kcal/mol along the reaction coordinate to the dissociated products.

(2) ORMAS-PT correctly reproduces the MRMP potential energy surface along the symmetric and anti-symmetric dimer buckling modes for a $Si_{15}H_{16}$ cluster. As the $Si_{15}H_{16}$ cluster geometry is perturbed along the symmetric and anti-symmetric buckling modes, the energy increases at both the ORMAS-PT and MRMP levels of theory. This indicates the symmetric structure is the global minimum.

(3) ORMAS-PT was applied to the oxoMn(salen) species to examine its performance with transition metal

complexes. The ORMAS-PT calculation reproduces the MRMP neutral singlet-triplet energy splitting and anionic doublet-quartet energy splitting with errors that are less than 0.6 kcal/mol.

(4) ORMAS-PT reproduces the MRMP ionization potentials for *trans*-polyacetylene polymers of various lengths. For the longer polymers, ORMAS-PT was shown to systematically converge to the MRMP results as the number of configurations used to construct the reference wavefunctions is systematically increased.

The ORMAS-PT method is an efficient approximation to the MRMP/MCQDPT level of theory. ORMAS-PT is able to attain a high level of accuracy and reduce the number of determinants required for a typical MRMP/MCQDPT by 1–2 orders of magnitude. It follows that ORMAS-PT reduces the system memory needed to handle large active spaces, and is therefore an efficient alternative to full CASSCF+PT calculations.

ACKNOWLEDGMENTS

This work was supported by a grant from the Air Force Office of Scientific Research. Enlightening discussions with Dr. Michael Schmidt, Dr. Joe Ivanic, and Prof. Klaus Ruedenberg are gratefully acknowledged.

[1]M. W. Schmidt and M. S. Gordon, Annu. Rev. Chem. **49**, 233 (1998).
[2]P. Seigbahn, A. Heiberg, B. Roos, and B. Levy, Phys. Scr. **21**, 323 (1980).
[3]K. Ruedenberg and K. R. Sundberg, in *Quantum Science*, edited by J.-L. Calais, O. Goscinski, J. Lindenberg, and Y. Öhrn (Plenum, New York, 1976), pp. 505–515; K. Ruedenberg, L. M. Cheung, and S. T. Elbert, Int. J. Quant. Chem. **16**, 1069 (1979); L. M. Cheung, K. R. Sundberg, and K. Ruedenberg, Int. J. Quant. Chem. **16**, 1103 (1979).
[4]R. Shepard, J. Phys. Chem. A **109**, 11629 (2005); R. Shepard, J. Phys. Chem. A **110**, 8880 (2006); R. Shepard and M. Minkoff, Int. J. Quantum Chem **106**, 3190 (2006); R. Shepard, M. Minkoff, and S. R. Brozell, Int. J. Quantum Chem **107**, 3203 (2007).
[5]S. R. White, Phys. Rev. Lett. **69**, 2863 (1992).
[6]D. Ghosh, J. Hachmann, T. Yanai, and G. K.-L. Chan, J. Chem. Phys. **128**, 144117 (2008).
[7]C. Møller and M. S. Plesset, Phys. Rev. **46**, 618 (1934).
[8]J. A. Pople, J. S. Binkley, and R. Seeger, Int. J. Quant. Chem. **10**, 1 (1976).
[9]J.-P. Malrieu, J.-L. Heully, and A. Zaitsevskii, Theor. Chim. Acta **90**, 167 (1995).
[10]P. M. Kozlowski and E. R. Davidson, J. Chem. Phys. **100**, 3672 (1994).
[11]E. R. Davidson and A. A. Jarzecki, *Recent Advances in Quantum Chemistry*, Vol. 4, edited by K. Hirao (World Scientific Publishing, Singapore, 1999), pp. 31–63.
[12]J. P. Finley and H. A. Witek, J. Chem. Phys. **112**, 3958 (2000).
[13]K. Andersson, P.-Å. Malmqvist, B. O. Roos, A. J. Sadlej, and K. Wolinski, J. Phys. Chem. **94**, 5483 (1990); K. Andersson, P.-Å. Malmqvist, and B. O. Roos, J. Chem. Phys. **96**, 1218 (1992); K. Andersson, Theor. Chim. Acta **91**, 31 (1995); H.-J. Werner, Mol. Phys. **89**, 645 (1996).
[14]J. Finley, P.-Å. Malmqvist, B. Roos, and L. Serrano-Andrés, Chem. Phys. Lett. **288**, 299 (1998).
[15]K. Hirao, Chem. Phys. Lett. **190**, 374 (1992); K. Hirao, Chem. Phys. Lett. **196**, 397 (1992); K. Hirao, Int. J. Quant. Chem. **S26**, 517 (1992).
[16]H. Nakano, J. Chem. Phys. **99**, 7983 (1993); H. Nakano, Chem. Phys. Lett. **207**, 372 (1993).
[17]P.-Å. Malmqvist, K. Pierloot, A. R. M. Shahi, C. J. Cramer, and L. Gagliardi, J. Chem. Phys. **128**, 204109 (2008); A. R. M. Shahi, C. J. Cramer, and L. Gagliardi, Phys. Chem. Chem. Phys. **11**, 10964 (2009).
[18]V. Sauri, L. Serrano-Andrés, A. R. M. Shahi, L. Gagliardi, S. Vancoillie, and K. Pierloot, J. Chem. Theory Comput. **7**, 153 (2011).
[19]H. Nakano, J. Nakatani, and K. Hirao, J. Chem. Phys. **114**, 1133 (2001). R. Ebisuzaki, Y. Watanabe, and H. Nakano, Chem. Phys. Lett. **442**, 164 (2007).
[20]H. Nakano, R. Uchiyama, and K. Hirao, J. Comput. Chem. **23**, 1166 (2002).
[21]V. N. Staroverov and E. R. Davidson, Chem. Phys. Lett. **296**, 435 (1998).
[22]J. Olsen, B. O. Roos, P. Jørgensen, and H. J. Aa. Jensen, J. Chem. Phys. **89**, 2185 (1988). P.-Å. Malmqvist, A. Rendell, and B. O. Roos, J. Phys. Chem. **94**, 5477 (1990).
[23]H. Nakano and K. Hirao, Chem. Phys. Lett. **317**, 90 (2000).
[24]J. Ivanic, J. Chem. Phys. **119**, 9364 (2003).
[25]J. Ivanic and K. Ruedenberg, Theor. Chem. Acc. **106**, 339 (2001).
[26]A. I. Panin and K. V. Simon, Int. J. Quant. Chem. **59**, 471 (1996). A. I. Panin and O. V. Sizova, J. Comput. Chem. **17**, 178 (1996).
[27]T. Fleig, J. Olsen, and C. M. Marian, J. Chem. Phys. **114**, 4775 (2001).
[28]Y. G. Khait, J. Song, and M. R. Hoffmann, Int. J. Quant. Chem. **99**, 210 (2004).
[29]J. Ivanic J. (unpublished)
[30]J. M. Rintelman, M. S. Gordon, G. D. Fletcher, and J. Ivanic, J. Chem. Phys. **124**, 034303 (2006).
[31]B. O. Roos, P. Linse, P. E. M. Siegbahn, and M. R. A. Blomberg, Chem. Phys. **66**, 197 (1982).
[32]M. S. Gordon and M. W. Schmidt, *Theories and Applications of Computational Chemistry, the First Forty Years*, edited by C. Dykstra, G. Frenking, K. S. Kim, and G. E. Scuseria (Elsevier, Amsterdam, 2005), pp. 1167–1189; M. W. Schmidt, K. K. Baldridge, J. A. Boatz, S. T. Elbert, M. S. Gordon, J. J. Jensen, S. Koseki, N. Matsunaga, K. A. Nguyen, S. Su, T. L. Windus, M. Dupuis, and J. A. Montgomery, J. Comput. Chem. **15**, 1347 (1993).
[33]R. Krishnan, J. S. Binkley, R. Seeger, and J. A. Pople, J. Chem. Phys. **72**, 650 (1980).
[34]FORS/CASSCF(6,9) 6-311G++(3df,3dp)
[35]T. H. Dunning, J. Chem. Phys. **90**, 1007 (1989); D. E. Woon and T. H. Dunning, J. Chem. Phys. **98**, 1358 (1993).
[36]J. Ivanic, J. R. Collins, and S. K. Burt, J. Phys. Chem. A **108**, 2314 (2004).
[37]R. Ditchfield, W. J. Hehre, and J. A. Pople, J. Chem. Phys. **54**, 724 (1971); W. J. Hehre, R. Ditchfield, and J. A. Pople, J. Chem. Phys. **56**, 2257 (1972); P. C. Hariharan and J. A. Pople Theor. Chim. Acta. **28**, 213 (1973); M. M. Fancl, W. J. Pietro, W. J. Hehre, J. S. Binkley, M. S. Gordon, D. J. Defrees, and J. A. Pople, J. Chem. Phys. **77**, 3654 (1982); V. A. Rassolov, J. A. Pople, M. A. Ratner, and T. L. Windus, J. Chem. Phys. **109**, 1223 (1998).
[38]J. Ivanic, J. Chem. Phys. **119**, 9377 (2003).
[39]Timing performed on two dual-quad core Intel Xeon R5420 nodes.
[40]K. Kimura, S. Katsumata, Y. Achiba, T. Yamazaki, and S. Iwata, *Handbook of HeI Photoelectron Spectra of Fundamental Organic Molecules* (Halsted Press, New York, 1981); T. J. Cave and E. R. Davidson, J. Phys. Chem. **92**, 2173 (1988); R. J. Cave and E. R. Davidson, J. Phys. Chem. **92**, 614 (1988); M. Beez, G. Bieri, H. Bock, and E. Heilbronner, Helv. Chim. Acta **56**, 1028 (1973); E. E. Astrup, H. Bock, K. Wittel, and P. Heimbach, Acta Chem. Scand. Ser. A **29**, 827 (1975); T. B. Jones and J. P. Maier, Int. J. Mass. Spectrom. Ion. Phys. **31**, 287 (1979).